The Astrophysical Journal, 769:120 (9pp), 2013 June 1 doi:10.1088/0004-637X/769/2/120

IDENTIFICATION OF FIVE INTERACTING BINARIES IN THE GALACTIC BULGE SURVEY

C. T. Britt[1,8], M. A. P. Torres[2,3], R. I. Hynes[1,8], P. G. Jonker[2,3,4], T. J. Maccarone[5], S. Greiss[6], D. Steeghs[3,6], P. Groot[4,7], C. Knigge[5], A. Dieball[5], G. Nelemans[4], V. J. Mikles[1], and L. Gossen[1,8]
[1] Department of Physics and Astronomy, Louisiana State University, Baton Rouge, LA 70803-4001, USA
[2] SRON, Netherlands Institute for Space Research, Sorbonnelaan 2, 3584-CA Utrecht, The Netherlands
[3] Harvard-Smithsonian Center for Astrophysics, 60 Garden Street, Cambridge, MA 02138, USA
[4] Department of Astrophysics/IMAPP, Radboud University Nijmegen, P.O. Box 9010, 6500-GL Nijmegen, The Netherlands
[5] School of Physics and Astronomy, University of Southampton, Hampshire SO17 1BJ, UK
[6] Astronomy and Astrophysics, Department of Physics, University of Warwick, Coventry CV4 7AL, UK
[7] Cahill Center for Astronomy and Astrophysics, California Institute of Technology, 1200 East California Boulevard, Pasadena, CA 91125, USA
Received 2012 October 23; accepted 2013 April 19; published 2013 May 14

ABSTRACT

We present optical light curves, spectroscopy, and classification of five X-ray sources in the Chandra Galactic Bulge Survey (CXOGBS J174009.1−284725 (CX5), CXOGBS J173935.7−272935 (CX18), CXOGBS J173946.9−271809 (CX28), CXOGBS J173729.1−292804 (CX37), CXOGBS J174607.6−261547 (CX561)). These objects were selected based on bright optical counterparts which were quickly found to have emission lines in their optical spectra. This paper presents an illustration of GBS optical follow-up, targeting emission line objects. Of these five objects, four exhibit photometric variability in the Sloan r' band. CX5 shows a tentative period of 2.1 hr and is clearly an intermediate polar (IP). CX28 and CX37 both exhibit flickering with no clear period. Both are also suggested to be IPs. CX18 was observed to undergo two dwarf nova outbursts. Finally, CX561 shows no detectable variability, although its characteristics would be consistent with either a quiescent low-mass X-ray binary or cataclysmic variable.

Key words: binaries: close – novae, cataclysmic variables – stars: dwarf novae – stars: emission-line, Be – surveys – X-rays: binaries

1. INTRODUCTION

The most comprehensive Galactic X-ray surveys of faint sources have focused on the Galactic center or on globular clusters. Surveys of the Galactic center carry the advantage of high source density (Muno et al. 2003), but also the disadvantages for optical follow-up of high crowding and A_V on the order of 30 mag. Together, those disadvantages make the determination of optical or infrared counterparts to X-ray sources in the Galactic center very difficult (Mauerhan et al. 2009). Establishing an optical/infrared counterpart is a necessary first step for characterizing the properties of the X-ray emitting objects. This characterization is done through a combination of the ratio of X-ray to optical luminosities, detection of ellipsoidal modulations of the companion, and optical and infrared spectroscopy. Studies of globular clusters avoid the problem of high extinction, but the crowding problem is even more severe. Also, X-ray binary (XRB) formation in globular clusters is dominated by dynamical processes, so they do not provide a probe of binary evolution in the field.

The Galactic Bulge Survey (GBS) is intended to avoid as much as possible the problems of crowding and extinction present in previous surveys of the Galactic center, while giving up as little as possible in the way of number of sources (Jonker et al. 2011). The GBS makes use of both optical and X-ray imaging of two $6^\circ \times 1^\circ$ strips located $1^\circ.5$ above and below the Galactic plane, cutting out the region with $|b| < 1^\circ$ to avoid copious amounts of dust in the Galactic plane. Other surveys, such as the ChaMPlane survey of bright X-ray sources, are also having some success in identifying sources along the plane and in low extinction windows (Servillat et al. 2012; van den Berg et al. 2009). The GBS is a shallower survey than others, with exposures of 2 ks (Jonker et al. 2011). This was done because deeper observations would pick up disproportionately more cataclysmic variables (CVs) than XRBs and also would overshoot the ability to perform optical spectroscopy on candidate counterparts (Jonker et al. 2011).

There are multiple goals to be achieved in such a census of X-ray sources (Jonker et al. 2011). We aim to greatly expand the known number of Galactic XRBs. By increasing the number of known low-mass X-ray binaries (LMXBs), we are bound to correspondingly increase the number of LMXBs for which mass determinations are possible. Identification of source class types is another main goal of the GBS because it allows constraints to be placed on binary evolution models by comparing observed source class numbers to the predictions of population synthesis models. Such models are widely divergent in their predictions (Ivanova et al. 2005; Kalogera 1999; Pfahl et al. 2003). Underlying these predictions are assumptions concerning the common envelope phase of binary evolution (Taam & Sandquist 2000). This paper presents the first few sources to be identified in the GBS as new interacting binaries.

We expect to find a large number of CVs in the survey, both with and without strong magnetic fields (Jonker et al. 2011). In the absence of a strong magnetic field, the white dwarf (WD) rotation period is not tidally locked to the binary orbital period (unlike the rotation period of the companion), the magnetic pressure never dominates the accretion flow, and an accretion disk can form. While these systems produce X-rays, the boundary layer in high accretion rate systems has a high optical depth that quenches X-ray emission, reprocessing it into UV light (Warner 2003). Non-magnetic CVs detected by the GBS are most likely quiescent CVs, where the amount of energy released as X-ray radiation is roughly two orders

[8] Visiting astronomer, Cerro Tololo Inter-American Observatory, National Optical Astronomy Observatory, which are operated by the Association of Universities for Research in Astronomy, under contract with the National Science Foundation.

Table 1
Differentiating Source Classes

Category	$\frac{F_x}{F_{\rm Opt}}$	$\frac{\rm EW(He\,I\,4471)}{\rm EW(H\beta)}$	$\frac{\rm EW(He\,I\,6678)}{\rm EW(H\beta)}$	$\frac{\rm EW(He\,II\,4686)}{\rm EW(H\beta)}$	Possible Variability	References
CV	0.01–1	0.22 ± 0.09[a]	0.1–0.5	<0.4[b]	Flickering, sinusoidal, ellipsoidal, DN	1, 2, 3, 11, 13
IP	0.1–10	0.17 ± 0.04[a]	0.1–0.5	>0.4[b]	Flickering plus reprocessed X-ray pulsation, sometimes DN	1, 2, 3, 11, 12
qLMXB (NS)	0.1–1	Nondetected[c]	0.12[c]	Nondetected[c]	Flickering, ellipsoidal, flares on timescale of tens of minutes or longer	7, 8
qLMXB (BH)	0.01–0.1	Nondetected[c]	0.12[c]	Nondetected[c]	Flickering, ellipsoidal, flares on timescale of tens of minutes or longer	5, 7, 8
LMXB	$\geqslant$100	$\leqslant$0.1[c]	0.3[c]	0.8[c]	Flickering, disk dominated, outbursts on timescale of a week to months, reprocessed thermonuclear bursts in case of NS primaries	4, 6, 9, 10

Notes.
[a] Average and standard deviation of reported EW ratios in Echevarria (1988).
[b] For systems where EW(Hβ)> 20 Å. This is not a definitive test, as it is based on tens of systems. The defining characteristic of IPs is an X-ray spin period for the WD that is less than the orbital period. Our X-ray observations are too shallow to permit detections of a spin period in most cases.
[c] Reported values are the average of observed EW ratios for the systems A0620-00 and V404 Cyg in quiescence and outburst, respectively.
References. (1) Warner 2003; (2) Echevarria 1988; (3) Silber 1992; (4) Hynes et al. 2004; (5) Zurita et al. 2003; (6) Remillard & McClintock 2006; (7) Marsh et al. 1994; (8) Menou et al. 1999; (9) Lasota 2001; (10) Casares et al. 1991; (11) Grindlay 1999; (12) Shara et al. 2005; (13) Grindlay 2006.

of magnitude less than the optical light from the system ($L_X/L_{\rm Opt} \sim F_X/F_{\rm Opt} \sim 1/100$), though it can be higher in systems with higher accretion rates (up to $\dot{M} \approx 10^{16}\,{\rm g\,s^{-1}}$). In general, $F_X/F_{\rm Opt}$ is correlated with both He II 4686 and Hβ emission, but more strongly with He II 4686 (Grindlay 1999).

A stronger magnetic field can lift material in accretion curtains off of the disk and funnel the material onto the magnetic pole. If the field is not strong enough to lock the WD's spin to the orbital period of the system, then it is called a DQ Her system or an intermediate polar (IP). Magnetic WD systems can produce a great deal more X-ray light than ordinary CVs, with $F_X/F_{\rm Opt} \sim 1$ (Warner 2003; Patterson 1994). In IPs, since the magnetic pole of the WD is likely not aligned with the spin axis, the bright accretion spot forms a beam (Patterson 1994). X-ray light from IPs is therefore pulsed on the rotation period of the WD. Some of this beam will hit structures orbiting the WD, which reprocess the X-ray light. In the optical, therefore, the period for reprocessed light is often observed. This is called the "orbital sideband" period, and is given by $\omega_{\rm Sideband} = \omega_{\rm Spin} - \Omega_{\rm Orb}$.

When the magnetic field of the WD is strong enough, it can lock the WD to the companion star, so that $P_{\rm Spin} = P_{\rm Orb}$, and funnel material to the magnetic pole of the WD directly from L1. These are called AM Her systems, after the proto-typical example, or polars.

Active Galactic LMXBs are some of the brightest X-ray sources in the sky, with examples including the brightest persistent X-ray source, Sco X-1. The ratio of X-ray to optical flux for such systems is on the order of 100 or more ($F_X/F_{\rm Opt} \geqslant 100$). When these systems enter quiescence, the X-ray flux drops significantly more than the optical light, resulting in a flux ratio closer to order unity for neutron star (NS) systems. Quiescent LMXBs (qLMXBs) with a black hole (BH) primary are less luminous in the X-ray than NS systems, which is thought to be a result of heated material falling beyond the event horizon of a BH before radiation can escape, whereas heated infalling material on the surface of an NS can eventually radiate the energy away (Narayan et al. 1997; Garcia et al. 2001; Hameury et al. 2003; Narayan & McClintock 2008). Another scenario is that the energy escapes the system through jets in BH systems (Fender et al. 2003). The qLMXBs we expect to find in the GBS have not gone through a recent outburst cycle; we are searching for quiescent systems, not following systems into quiescence from outburst. It is possible, therefore, that the quiescent properties of systems in the GBS are different from known qLMXBs.

Some counterparts to GBS sources are visible in the Optical Gravitational Lensing Experiment data (Udalski et al. 2012). Crowding in these fields is high enough that sources should be treated with care, as the odds of a chance alignment of the X-ray position with an unrelated variable star are non-negligible.

We provide a rough rubric to differentiate between these compact binary systems in Table 1. Values are drawn from existing literature on each category, and are based on a limited number of well-observed CVs and only one BH qLMXB and one NS qLMXB. Though they are representative of the characteristics of similar systems, they should be taken with care. Often, the optical flux in existing literature refers to V-band measurements. Our photometry consists of Sloan r' observations, and will henceforth report flux values as $F_{r'}$ rather than $F_{\rm Opt}$. The difference in these broadband measurements depends on the spectral energy distribution of the source, but is small compared to the difference with the X-ray flux.

In this paper, we examine the first five accreting binaries identified in the GBS by means of long-slit optical spectroscopy and optical photometry.

2. DATA REDUCTION

2.1. Spectroscopy

We targeted the five objects presented in this paper during our spectroscopic campaigns to identify and classify the optical counterparts to GBS X-ray sources. Data were acquired between 2010 July 8 and July 11 under program 085.D-0441(C) with the New Technology Telescope (NTT) equipped with the ESO Faint Object Spectrograph and Camera (EFOSC2). These five sources are selected from among the targets of the 2010 NTT observations as the only sources showing strong emission lines in the spectra. Results on the other sources will be presented elsewhere. The observations were performed using grism #13 and a 1″ wide slit that provided an instrumental spectral resolution of ∼17 Å (FWHM) in the $\lambda\lambda$ = 3700–9200 Å wavelength range. Integration times ranged between 400 s and 900 s. HeAr arc lamp and flat-field exposures were taken after each target observation. Additionally, on 2011 April 2,

two consecutive 875 s spectra of the optical counterpart to CX28 were obtained with the Visible Multi Object Spectrograph (VIMOS; Le Fèvre et al. 2003) mounted on the ESO Very Large Telescope under program 085.D-0441(A). The MR red grism and a 1″ wide slit were used, achieving a spectral resolution of 10 Å FWHM and a wavelength range of $\lambda\lambda = 4600$–10000 Å.

The EFOSC2 data set was bias and flat-field corrected with standard IRAF[9] routines. The spectra were extracted with the IRAF KPNOSLIT package. The pixel-to-wavelength calibration was derived from cubic spline fits to HeAr arc lines. The rms deviation of the fit was <0.1 Å. Checks for the stability of the wavelength calibration were made using the atmospheric [O I] 5577.34 and 6300.3 Å sky lines. In this way, we estimated an accuracy in the wavelength calibration of <0.5 Å. The VIMOS spectra of CX28 were reduced with the VIMOS ESO pipeline version 2.6.2 (Izzo et al. 2004) and extracted using IRAF (see M. A. P. Torres et al. 2013, in preparation, for details).

2.2. Optical Photometry

2.2.1. Blanco Photometry

We acquired eight nights of photometry, from 2010 July 12 to 18, with the Blanco 4.0 m telescope at the Cerro Tololo Inter-American Observatory (CTIO). Using the Mosaic-II instrument, we observed the 9 deg^2 area containing two-thirds of the X-ray sources identified by the GBS (Jonker et al. 2011). Multiple Sloan r'-band exposures with an integration time of 120 s of 45 overlapping fields were taken to cover the area. Typical seeing for the run was around 1″. The order in which the fields were cycled was randomized to minimize aliasing caused by regular sampling. The data were reduced via the NOAO Mosaic Pipeline (Shaw 2009), which also added a world coordinate system (WCS) to the images.

The NOAO pipeline searches for instrumental artifacts in the image, corrects for cross talk between CCDs, applies a pupil ghost correction for light reflecting from the filter to the back surface of the corrector then back through the filter, applies bias and flat-field corrections, and calibrates WCS for each image based on USNO-B1 stars in the field. Dark current calibrations are unnecessary. A detailed explanation of each procedure can be found in chapter 2 of the NOAO Data Handbook (Shaw 2009).

Photometry on the five sources with NTT spectra showing emission lines was done using Alard's image subtraction routine, ISIS, described in detail in Alard & Lupton (1998) and Alard (2000). ISIS works by using a reference image which it then convolves with a kernel in an effort to match a subsequent image of the same field. The subsequent image is then subtracted from the convolved reference image. Stars that do not vary in magnitude should subtract cleanly, so the subtracted image is clear of non-variable objects. Therefore, any residual flux is due to an inherent change in the brightness of a source. To perform photometry on the subtracted image, the point-spread function (PSF) for each image is scaled by χ^2 minimization to represent the change in flux from the reference image. The error bars are calculated through χ^2 minimization as well. Systematic errors in determining the PSF across each image are not accounted for, however. In most cases, these errors are quite small, as demonstrated by cleanly subtracted frames. In order to save computation time, small cutouts of the full Mosaic images, 401×401 pixels or $104'' \times 104''$, were taken around each object for processing.

Once a light curve was in hand, if a source showed significant variability, periodograms were created using the Lomb–Scargle statistic in an effort to search for periodicities. Since ellipsoidal variations have two maxima and minima in a single orbital period, we also check periods twice as long as prominent peaks on a periodogram. We also consider both aliases and harmonics, as higher harmonics can sometimes show up at a higher power than the fundamental frequency.

At present, we lack photometric standard observations for these sources in r', so all apparent magnitudes cited here are scaled to nearby stars in the USNO-B1 catalog and are to be used with caution until secondary standards are established for all Mosaic fields. The magnitude scaling, which is a pipeline calibration product, carries an estimated uncertainty of ±0.5 mag for each source. This is quite adequate for estimating X-ray to optical flux ratios.

2.2.2. SMARTS Photometry

We also used the SMARTS Consortium's 1.3 m at CTIO to gather further optical data for CX18 and CX37 with the ANDICAM instrument. Exposures were taken with a 250 s integration time in the R-band filter. Typical seeing was 1″. These data were reduced via pipeline, which added overscan corrections, bias corrections, and applied dark current exposures and dome flats taken by the queue observer. Photometry was performed with ISIS as described above.

2.2.3. Swope Photometry

For objects showing suspected rapid variability, we observed them from 2011 June 21 through 2011 June 27 at the 1.0 m Henrietta Swope telescope with the SITe #3 CCD at Las Campanas Observatory (LCO). We observed in the Gunn r filter, and tracked the objects to confirm periods found with Mosaic-II data and provide more complete phase coverage of each source. Exposure times varied from two to five minutes depending on the brightness of the counterpart. Typical seeing was ∼1.3″. These data were reduced using standard IRAF procedures in the CCDRED package with bias and flat-field frames taken each night; photometry was performed with ISIS as above.

2.2.4. Extinction Corrections

To correct for extinction due to dust, in this paper we use A_K and $E(B-V)$ values from Gonzalez et al. (2012) and the extinction law in Cardelli et al. (1989). We transform these to r' using filter property values in Schlegel et al. (1998). To determine X-ray absorption, we use the relation $N_H = 5.8 \times 10^{21}\ \mathrm{cm}^{-2}\ E(B-V)$ found by Bohlin et al. (1978). Predehl & Schmitt (1995) find a value of $N_H = 1.79 \times 10^{21}\ \mathrm{cm}^{-2}\ A_V$, which, using the extinction law in Cardelli et al. (1989), does not differ substantially from the findings of Bohlin et al. (1978). For CX5, where there are previously reported X-ray spectral properties, we use those. For other suspected IPs, we assume a model spectra of bremsstrahlung radiation with $kT = 25$ keV, while for the remaining sources we assume a power-law spectral shape of $\Gamma = 2$ (Jonker et al. 2011). It is important to note that these extinction values are upper limits along the line of sight to the red clump stars used in Gonzalez et al. (2012) rather than extinctions based on each object's actual reddening. Since extinction has a larger effect on optical wavelengths than X-rays, using these extinction values provides a lower limit to

[9] IRAF is distributed by the National Optical Astronomy Observatory, which is operated by the Association of Universities for Research in Astronomy (AURA) under cooperative agreement with the National Science Foundation.

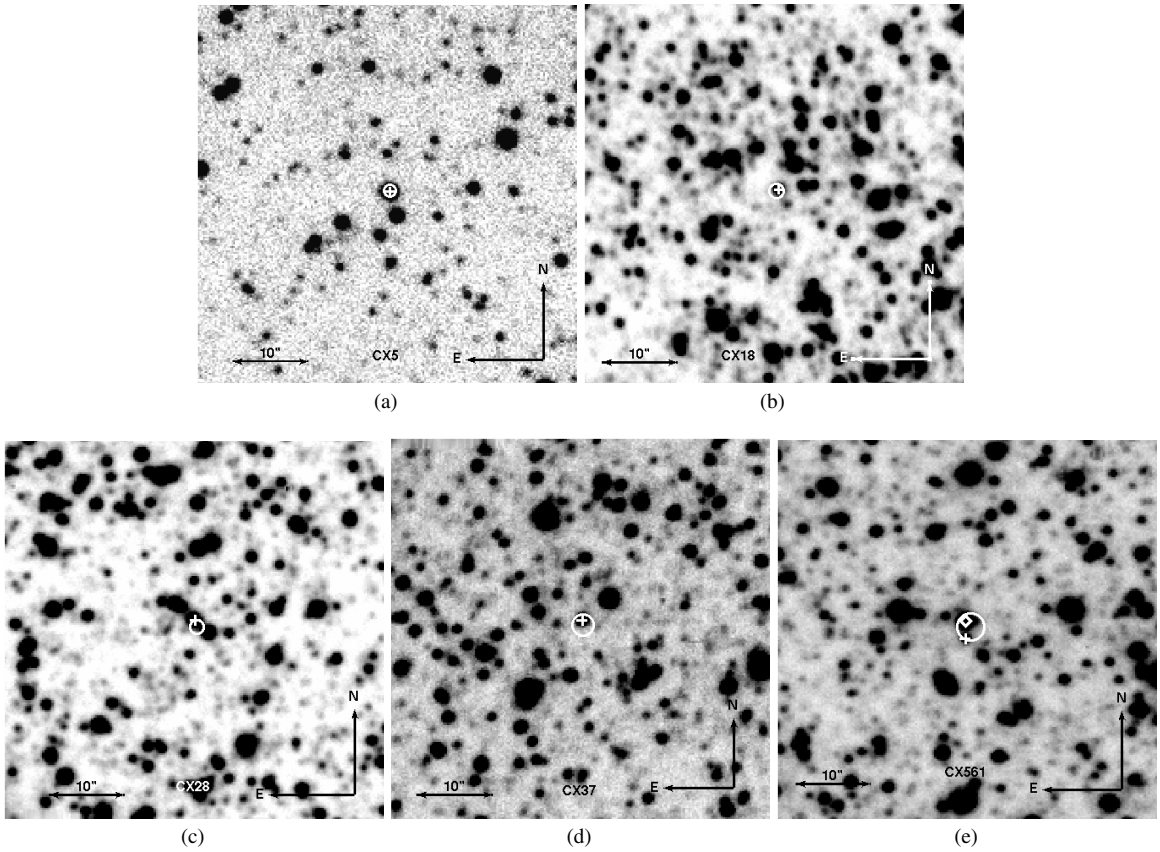

(a) (b) (c) (d) (e)

Figure 1. Finder charts for the five listed GBS sources. The 3σ X-ray position is plotted with a white oval, while the optical companion is marked with a white cross: (a) CX5, (b) CX18, (c) CX28, (d) CX37, (e) CX561, with a nearby eclipsing binary system marked with a white diamond. In all charts, north is up and east is left.

the X-ray to optical flux ratio. This could be quite extreme, since the CVs are likely in the foreground.

3. RESULTS

Figure 1 shows a cutout of the Blanco image around each X-ray source. Table 2 presents the emission line parameters for each source, while the spectra themselves are in Figure 2. Light curves of Mosaic-II data are shown in Figure 3, while follow-up light curves are presented in Figure 4. Of the five objects presented, one shows an eclipse, one shows a possible two hour period, two display aperiodic flickering, and one is not variable.

3.1. CXOGBS J174009.1−284725 (CX5)

This source is also known as AXJ1740.1−2847 and shows an X-ray period of 729 s (Sakano et al. 2000). In an IP interpretation, this pulse period is the spin of the WD. Sakano et al. (2000) fit the X-ray spectrum of CX5 to a power law of index $\Gamma = 0.7 \pm 0.6$ with $N_{\rm H} = 2.5^{+2.9}_{-1.8} \times 10^{22}$ cm^{-2}. Kaur et al. (2010) find $N_{\rm H} = 1.0 \pm 0.2 \times 10^{22}$ cm^{-2} with $\Gamma = 0.5 \pm 0.1$. Kaur et al. (2010) also report the presence of Fe emission. Its optical spectrum shows He II emission lines, which rules out a qLMXB interpretation. The ratio of equivalent widths between He II λ4686 and Hβ is 2.3, which is suggestive of a magnetic CV. Using the value in Kaur et al. (2010) for $N_{\rm H}$ to calculate extinction and absorption, we find the ratio of X-ray to optical flux is $F_x/F_{r'} \sim 0.4$, which is consistent with an IP, CV, or qLMXB. Assuming a distance of 1 kpc yields $L_X = 3 \times 10^{32}$ erg s^{-1}, which is within errors of previously reported values for this source.

This source shows a variability of 0.3 mag in our Mosaic-II data, the light curves of which are shown in Figure 3. The Mosaic-II observations for this source do not show a well-defined periodicity. We obtained six hours of intermittent photometry with the Henrietta Swope Telescope at LCO from 2011 June 22 and turned to this source again on 2011 June 27. We see evidence of a 125 minute period in the optical (see Figure 4). The Mosaic-II observations do not show evidence of this period. Using $P_{\rm spin} \sim 0.1\ P_{\rm Orb}$ as the apparent peak of the distribution of known IPs (Scaringi et al. 2010), one expects a 729 s pulse period to result in a roughly 2 hr orbital period, lending credibility to identifying the 125 minute period as the orbital period. The previously detected X-ray period of 729 s, hard X-ray spectrum with Fe emission, strong He II emission, and possible 125 minute orbital period ($\sim 10 \times P_{\rm spin}$) point to CX5 being an IP when taken together.

3.2. CXOGBS J173935.7−272935 (CX18)

This object is noted as a variable star in Terzan & Gosset (1991). The optical spectrum of CX18 shows He I and Balmer emission. In the Mosaic-II data, this source brightens by 1.6 mag over the course of six days. Follow-up data from SMARTS, which can be seen in Figure 3, clearly show a similar rise of 3 mag followed by an exponential decay and a flat quiescent state after the outburst. In two observations spaced out by several months, we caught two of these outbursts, suggesting a high recurrence rate. This source appears to be a CV undergoing dwarf nova (DN) outbursts, which is in agreement with Udalski et al. (2012), who find DN outbursts with a recurrence time

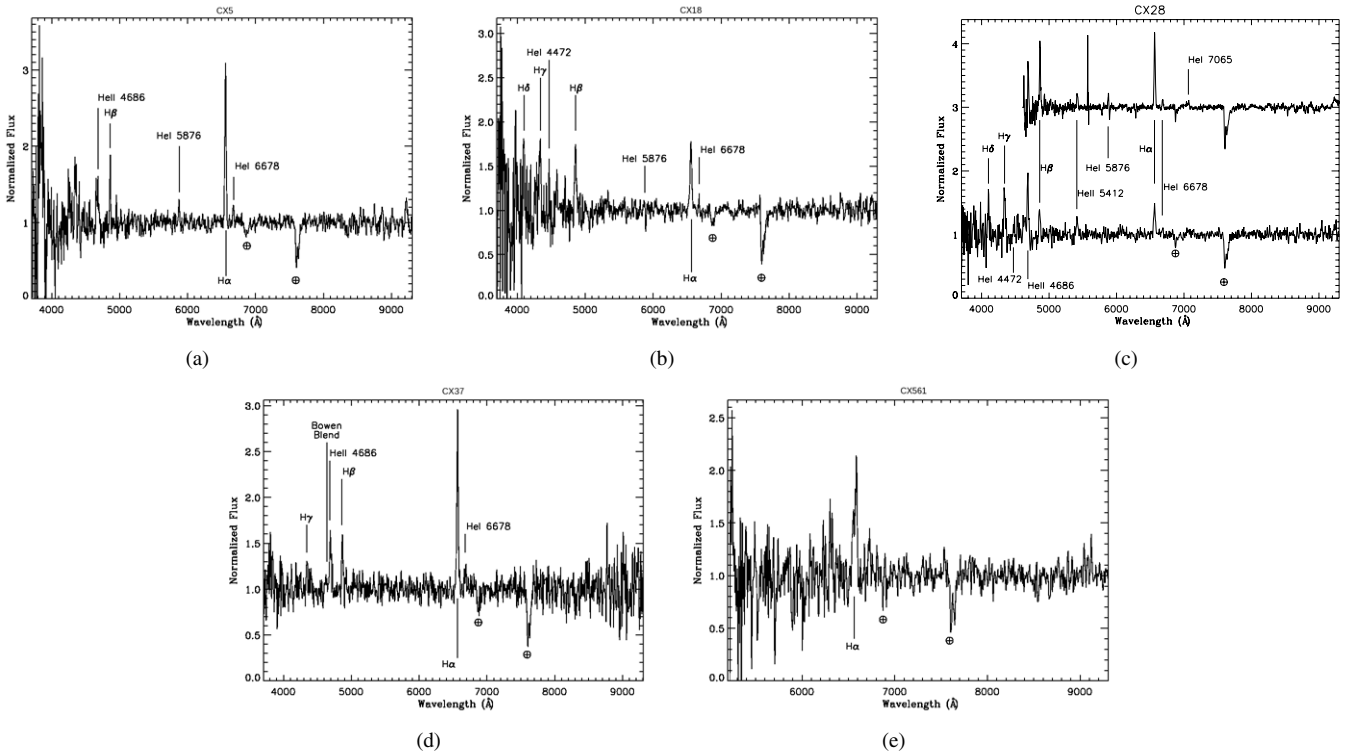

Figure 2. (a) Two epochs of the NTT spectrum for CX5. (b) Two epochs of the NTT spectrum for CX18. (c) The bottom epoch is from NTT observations of CX28, while the top comes from the VIMOS instrument on the VLT. (d) The NTT spectrum for CX37. (e)The NTT spectrum for CX561.

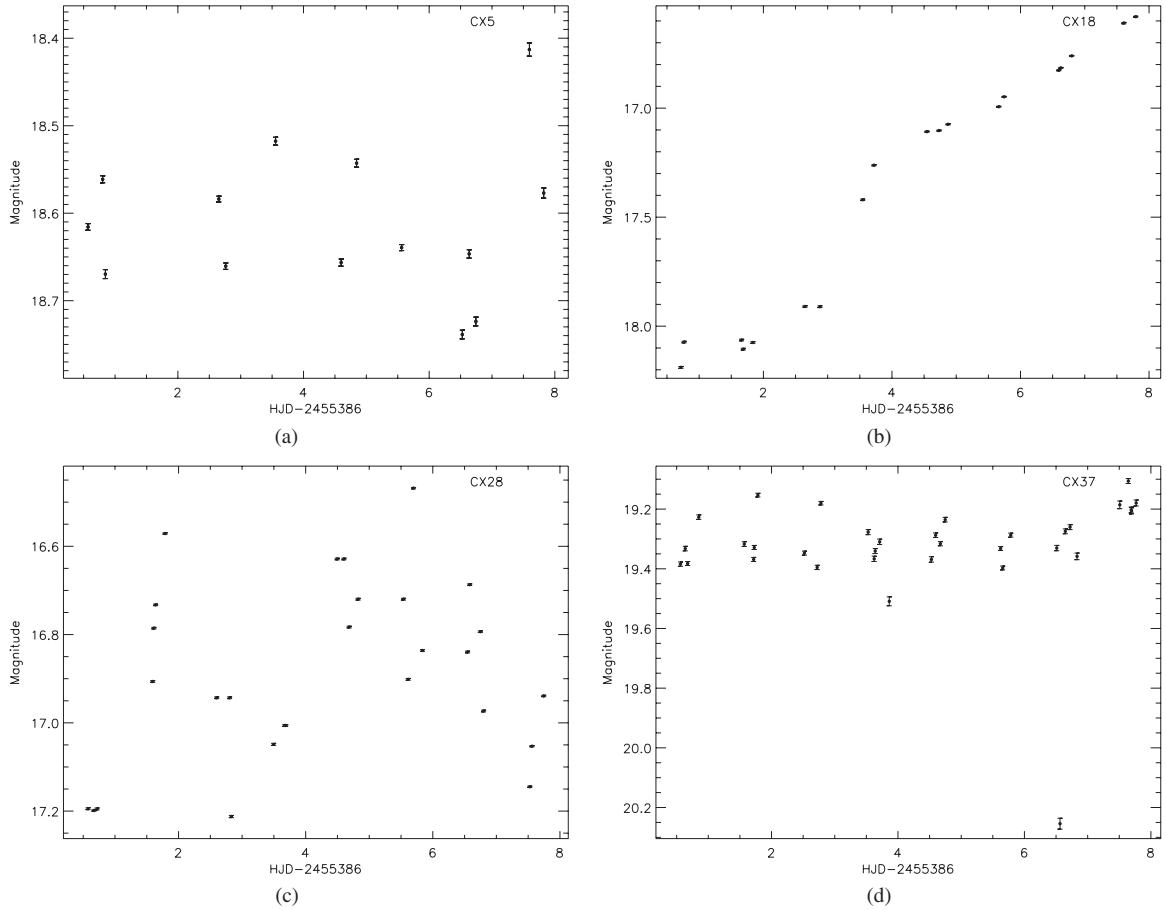

Figure 3. (a) Light curve of CX5 from Mosaic-II data. (b) Light curve of CX18 from Mosaic-II data, showing a rise of 1.5 mag over six days. (c) Blanco Mosaic-II light curve of CX28. (d) Blanco Mosaic-II light curve of CX37, showing an eclipse 4.39 times the standard deviation of the light curve below the median magnitude.

Table 2
Spectral Properties of Optical Counterparts

CX ID	Line	Epoch	λ_{Obs} (Å)	Radial Velocity (km s^{-1})	EW (Å)	FWHM (Å)
5	He II 4686	1	4682.7	-190 ± 70	-30 ± 4	23
	Hβ	1	4863.9	160 ± 10	-13 ± 1	12
	He I 5876	1	5879.3	190 ± 20	-4.9 ± 0.3	<14[b]
	Hα	1	6565.3	112 ± 5	-50 ± 2	13
	He I 6678	1	6681.1	130 ± 20	-4.9 ± 0.2	9
18	Hδ	1	4096.4	-390 ± 90	-18 ± 3	18
	Hγ	1	4338.8	-110 ± 80	-25 ± 2	19
	He I 4471	1	4470.3	-80 ± 20	-9 ± 2	<11[b]
	Hβ	1	4858.8	-160 ± 50	-25 ± 1	21
	He I 5876	1	5874.4	-60 ± 150	-3 ± 1	19
	Hα	1	6562.1	-30 ± 10	-25 ± 1	21
	He I 6678	1	6680.2	90 ± 30	-2.6 ± 0.4	<11[b]
28	Hδ	1	4101.5	-20 ± 10	-15 ± 2	9
	Hγ	1	4340.4	-4 ± 10	-24 ± 2	19
	Bowen blend	1	4635.6		-12 ± 1	34
	He II 4686	1	4684.9	-50 ± 20	-22 ± 2	11
		2	4691.8	390 ± 30	-20 ± 2	
	Hβ	1	4858.9	-150 ± 20	-11 ± 1	9
		2	4866.1	290 ± 30	-24 ± 5	12
	He II 5412	1	5416.1	250 ± 20	-6.9 ± 0.6 1	17
		2	5418.1	360 ± 30	-4.9 ± 0.3	21
	He I 5876	1	5874.6	-50 ± 20	-1.4 ± 0.6	<11[b]
		2	5878.1	130 ± 20	-3.5 ± 0.3	11
	Hα	1	6563.2	20 ± 10	-13 ± 0.5	17
		2	6565.9	140 ± 10	-26.2 ± 0.3	16
	H I 6678	1	6683.3	230 ± 80	-1.9 ± 0.6	7
		2	6682.5	200 ± 20	-2.6 ± 0.2	7
37	Hγ	1	4347.0	450 ± 20	-7.5 ± 0.7	11
	Bowen blend	1	4626.9		-5.5 ± 0.2	28
	He II 4686	1	4694.9	590 ± 30	-16 ± 2	14
	Hβ	1	4871.1	600 ± 10	-14 ± 1	9
	Hα	1	6574.4	530 ± 10	-45 ± 2	12
561	Hα	1	6553.4, 6585.5[a]	$1030 \pm 30, -430 \pm 30$[a]	$-18 \pm 2, -31 \pm 2$[a]	
		1	6576.6	630 ± 40	-52 ± 5	46

Notes. Three of the five sources have observed spectra at multiple epochs. Line widths are reported for each epoch in which they are present. Two values separated by commas denote a double-peaked line; reported values are for each peak. The FWHM of the lines have been deconvolved with the resolution of the instrument, which is 17 Å for NTT spectra and 10 Å for the VIMOS spectrum listed as epoch 2 for CX28. Coordinates of counterparts are from USNO-B1 astrometry.

[a] Line is double peaked, center and EW given for each peak. Line is fit with a single Gaussian below.

[b] Line widths are upper limits.

around 100 days in Optical Gravitational Lensing Experiment data.

Using the $E(B-V)$ values from Gonzalez et al. (2012) yields an X-ray to optical flux ratio of the order of 1/10, which is consistent with previous observations of the ratio of X-ray to optical light of quiescent DNe (Verbunt et al. 1997). Most DNe are substantially closer than bulge distance, but even assuming that no absorption occurs, the unabsorbed ratio of X-ray to optical flux of the order of unity is within the range of ordinary CVs. DN outbursts can occur in both CVs and in IPs with sufficiently large disks. Many IPs show strong He II emission in their optical spectra (Edmonds et al. 1999). CX18 does not. The lack of He II lines combined with the comparatively strong X-ray emission indicates that this is a quiescent system at the time of the spectroscopy and argues against an IP interpretation.

3.3. CXOGBS J173946.9−271809 (CX28)

The optical spectrum shows Balmer and He I emission, which makes this a good CV candidate. There is also consistently strong He II emission with He II 4686/Hβ = 2 in the first epoch of observations and He II 4686/Hβ = 0.8 in the second, suggesting an IP. X-ray observations described in Jonker et al. (2011) show that the X-ray spectrum of CX28 is hard, ([2.5–8 keV] − [0.3–2.5 keV])/([0.3–8 keV]) = 0.5, which further supports an IP classification, though there are not enough

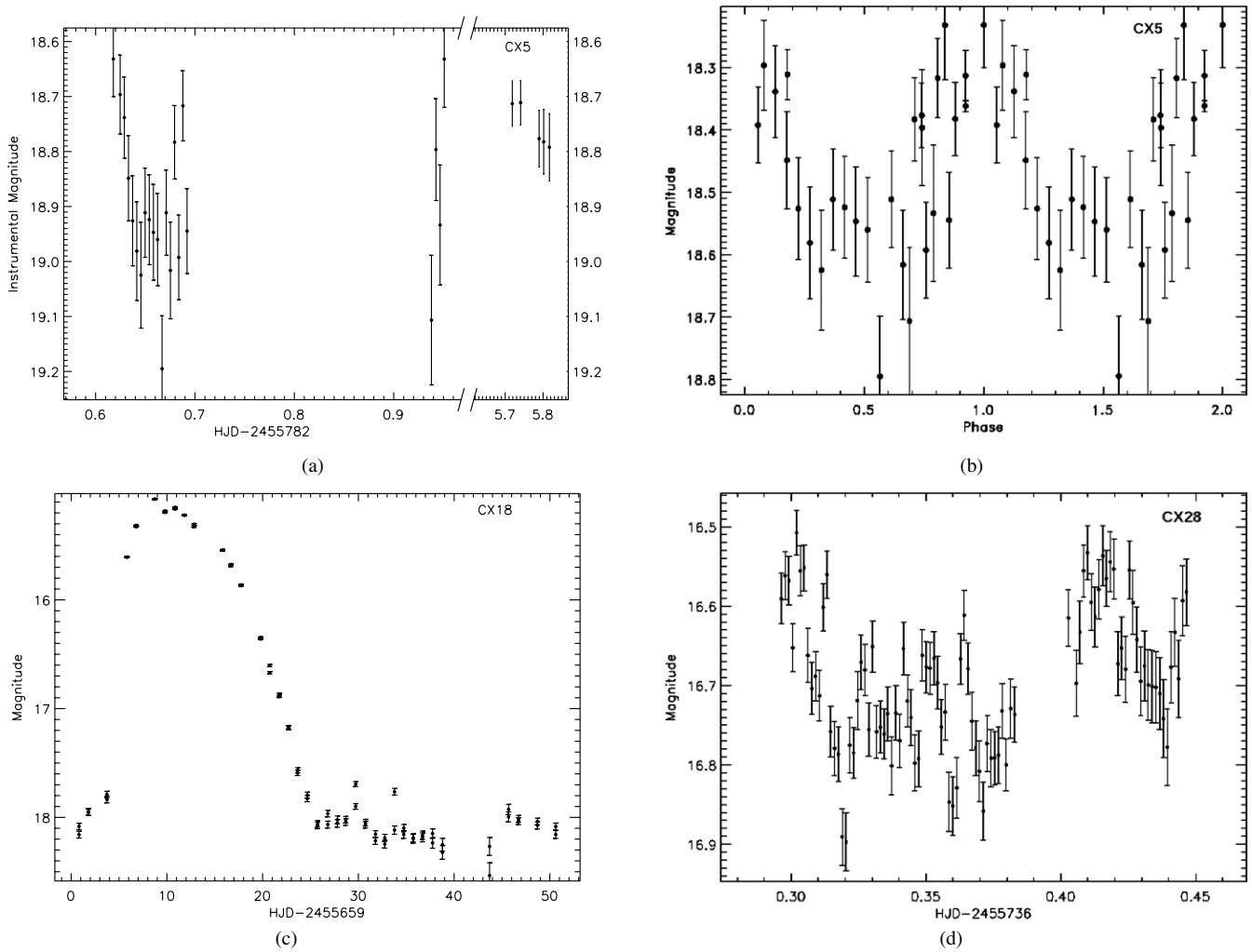

Figure 4. (a) Light curve of CX5 from the Swope 1.0 m data taken in the summer of 2011. (b) Swope light curve of CX5 folded on a 125 minute period with an arbitrary ephemeris. (c) Data collected with the SMARTS 1.3 m Andicam in the spring of 2011 confirm that CX18 is undergoing dwarf nova outbursts with a fast recurrence time. (d) CX28 Light curve from Henrietta Swope telescope at LCO.

photons in the 2 ks observation for a full spectral fit or for timing analysis. Unabsorbed $F_X/F_{r'} \sim 0.6$, which is consistent with IPs and CVs. This source cannot be a qLMXB based on the He II emission, and the X-ray strength is too weak for an active LMXB or accretion disk corona. The strength of the He II emission and hardness of the X-ray spectrum suggest that CX18 is an IP, though there are no observations of the defining IP characteristic of an X-ray spin period. The source varies by 0.7 mag, but is not demonstrably periodic in Mosaic-II data. Observations from 2011 June at the Swope telescope, shown in Figure 4(d), do not exhibit any period on timescales of minutes to an hour. There is some suggestion of a 2.76 hr period, but the observations do not extend long enough to bear this out as we do not cover multiple periods. If this is the real period, then flickering on top of the periodic changes could swamp the signal in our Mosaic-II observations. It is worth noting that this falls in the period gap for CVs and could be further evidence for an IP interpretation because the CV period gap is not observed in IPs. The changes in radial velocity (RV) observed between the VIMOS and NTT observations, shown in Table 2, are consistent with velocity variations in either the emitting regions or the motion of the disk around the mass of the system.

3.4. CXOGBS J173729.1−292804 (CX37)

The optical spectrum of CX37 shows Balmer, He I, and He II emission, meaning that the source is not a qLMXB. The relative strength of He I to Balmer lines is consistent with a WD primary, while the strong He II emission (He II 4686/Hβ = 1.1) rules out a qLMXB (see Table 1). Absorbed $F_X/F_{r'} \sim 5$, while adjusting for extinction lowers this value to a minimum of 1/16 at the bulge, which is consistent with CVs and IPs. There are 37 photons detected in the 2 ks *Chandra* observation of this source (Jonker et al. 2011), which is enough to reveal that the X-ray spectrum of CX37 is very hard, with ([2.5–8 keV] − [0.3–2.5 keV])/([0.3–8 keV]) = 0.9. In the Blanco data, CX37 shows non-periodic variability of amplitude 0.15 mag from the mean and evidence of an eclipse at least 0.9 mag deep, as shown in Figure 3(d). The other variations are largely due to flickering, as no significant periodic modulations are recovered from a periodogram. The lowest data point in the Mosaic-II light curve is 4.39 times the standard deviation of all the 34 observations, suggesting that it is indeed an eclipse rather than a random fluctuation from flickering. There is a second data point that is 2.64 times the standard deviation below the mean, which is likely a second eclipse. The

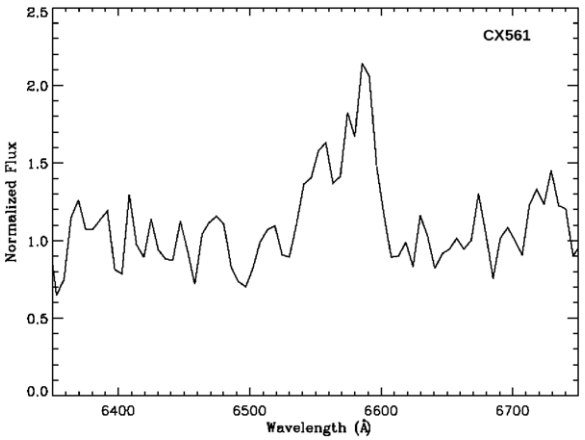

(a)

Figure 5. Zoom in on the double-peaked Hα line in the NTT spectrum of CX561, peaks separated by 30 Å or 1420 km s^{-1}, which implies a disk velocity of 710 km s^{-1}

eclipsing points are 2.7 days apart. Also, catching two eclipsing points out of 34 suggests that the eclipse lasts for $\sim 6^{+4}_{-3}$% of the period, which is not unusual for CVs (Sulkanen et al. 1981). Since the nearest observation to the eclipse is separated by only 1.25 hr, that suggests a maximum period of $\sim$21 hr, assuming the two points are from eclipses at the same phase. In 4.5 hr of observations with the Swope telescope at LCO (not shown), CX37 varies with no periodicity and with no visible eclipse. The LCO observations provide a lower bound to the orbital period, implying that the period is some fraction 2.7 days/n, $3 \leqslant n \leqslant 14$.

Each of the emission lines also exhibit large RVs, shown in Table 2, from 400 to 600 km s^{-1}. It is possible to produce offsets this high in low inclination and short-period magnetic systems.

The hardness of the X-ray spectrum together with the strong He II emission suggests an IP classification for CX37, but as with CX28, X-ray observations capable of detecting a spin period are necessary to make this classification definitively.

3.5. CXOGBS J174607.6−261547 (CX561)

The approximate r' magnitude of CX561 is 20.2. The only feature in this spectrum is Hα. As shown in Figure 5 and Table 2, the Hα emission line is split with peaks of unequal heights, suggesting significant contribution from a hotspot on the disk. The separation between the peaks is 1420 km s^{-1}, which is not high enough to rule out a CV interpretation (Szkody et al. 2002; Szkody & Henden 2005; Warner 2003). The center of the line profile is at 6576.5 Å, which suggests a velocity along our line of sight of 630 km s^{-1}. It is possible to produce these speeds for low inclination and short-period magnetic or nova-like WD systems if observed at the right phase. Natal kicks routinely produce LMXBs with systemic velocities on this order. There is no evidence of He I or He II lines in the spectrum, but the signal-to-noise ratio is so low that a typical amount of He I for a CV could be present and buried in the noise.

We have only five counts in the *Chandra* data for this source, so we cannot know the shape of the spectrum, but using the assumptions in Jonker et al. (2011) we find that $F_X/F_{r'}$ lies in the range of 1/50–1, depending on how much of the dust in the line of sight it lies behind. This is consistent with both CVs and qLMXBs. It is too X-ray bright compared to its optical emission to be a coronally active star, and Hα is not redshifted enough to suggest an active galactic nucleus as X-ray faint as CX561 is. Its absolute magnitude at a distance of 1 kpc would be consistent with quiescent CVs and qLMXBs depending on the donor star, and its absolute magnitude at a distance of 8 kpc is $M_{r'} \approx 1$, which is consistent with the brightest qLMXBs. At bulge distance, $L_X = 6 \times 10^{32}$ erg s^{-1}, which is consistent with both NS and BH qLMXBs, while $L_X = 5 \times 10^{30}$ erg s^{-1} for a distance of 1 kpc, which is consistent with BH qLMXBs and CVs. If the system is distant, then the X-ray to optical flux ratio is a bit low for an NS primary, but this cannot be ruled out for two reasons. First, the uncertainty in the ratio is quite high. With only five photons in the X-ray and no spectral information, and without photometric standards in the optical or an exact extinction measurement, this value could be off by an order of magnitude when uncertainties from all of these factors are considered. Also, if this is indeed a qLMXB with an NS primary, it has not undergone recent outbursts and could display different properties in quiescence than those systems that have been followed into quiescence from an active state.

CX561 showed no significant optical variability in the Mosaic-II data. There is, however, an eclipsing binary with r' magnitude 17.2 ± 0.5 with a 12.5 day period next to the emission line object. It is marked in the finder chart in Figure 1 with a white circle. It is this nearby variable that has been mistakenly identified as the counterpart by Udalski et al. (2012).

4. CONCLUSION

We have proposed identifications to the optical counterparts to four of the five initial GBS sources that show emission lines. Of these, one is a definite IP, one is a DN, and two others are good candidates for IPs. A summary of the X-ray and optical characteristics of each object can be found in Table 3. CX5 shows periodic X-ray behavior on the timescale of minutes, strong He II emission, a hard X-ray spectrum, a possible optical orbital period of $\sim 10\ P_{\rm spin}$, and an X-ray to optical flux ratio just less than unity, making an IP classification certain. CX18 shows He I and Balmer emission and two DN outbursts. CX28 and CX37 both show strong He II emission with hard X-ray spectra but are too faint in the X-ray to be XRBs, making them likely IPs. The fifth source, CX561, has an uncertain classification without further follow-up, though the double-peaked Hα line means it is a close binary that could either contain a WD or a BH as the compact object. It is not surprising that our large-field Mosaic-II observations did not isolate orbital sideband periods in the IPs which can be on the order of hundreds to thousands of seconds, but they were sufficient to determine the optical counterpart of identified X-ray sources and to identify eclipsing systems.

These results represent too small and biased a sample of the survey data to allow any conclusions to be drawn about the population of sources we are finding, but they are consistent with the expectations in Jonker et al. (2011). We will continue to identify new objects as counterparts are identified and classified.

This work was supported by the National Science Foundation under grant No. AST-0908789, by the Louisiana Board of Regents Fellowship, by the NAS/Louisiana Board of Regents grant NNX07AT62A/LEQSF(2007-2010) Phase 3-02. P.G.J. and M.A.P.T. acknowledge support from the Netherlands Organisation for Scientific Research, and the work of their student Oliwia Madj. This research has made use of NASA's Astrophysics Data System Bibliographic Services and of SAOImage DS9, developed by Smithsonian Astrophysical Observatory.

Table 3
Summary of X-ray and Optical Characteristics

CX ID	5	18	28	37	561
R.A. (J2000)	17 40 09.13	17 39 35.76	17 39 47.01	17 37 29.18	17 46 07.68
Decl. (J2000)	−28 47 25.7	−27 29 35.7	−27 18 08.7	−29 28 03.9	−26 15 49.1
X-ray flux (counts per 2 ks)	157	68	46	37	5
Absorbed F_x (erg cm^{-2} s^{-1})	2×10^{-12}	4×10^{-13}	4×10^{-13}	3×10^{-13}	4×10^{-14}
Unabsorbed F_x (erg cm^{-2} s^{-1})	4×10^{-12}	9×10^{-13}	6×10^{-13}	5×10^{-13}	7×10^{-14}
Absorbed $F_{r'}$ (erg cm^{-2} s^{-1})	2×10^{-12}	2×10^{-13}	6×10^{-13}	6×10^{-14}	3×10^{-14}
Unabsorbed $F_{r'}$ (erg cm^{-2} s^{-1})	1×10^{-11}	8×10^{-12}	3×10^{-11}	8×10^{-12}	3×10^{-12}
Unabsorbed $\log(\frac{F_x}{F_{r'}})$	−0.4[a]	0.3	−0.2	0.7	0.1
$\log(\frac{F_x}{F_{r'}})$ at bulge	...	−0.9	−1.7	−1.2	−1.6
$E(B-V)$ at bulge	1.7	1.6	1.6	2.0	1.8
$\frac{\text{He II } 4686}{\text{H}\beta}$	2.3	<0.1	2.0, 0.83	1.1	...
$\frac{\text{He I } 4471}{\text{H}\beta}$	...	0.4	...	...	...
$\frac{\text{He I } 6678}{\text{H}\beta}$	0.4	0.1	0.1	0.3	...
References	1, 2, 3, 5	4, 5	4, 5	3, 5	3, 5

Note.
[a] The value for $N_{\rm H}$ determined by Kaur et al. (2010) is used to calculate $E(B-V)$ and flux values for CX5. This likely somewhat overestimates reddening as some of the $N_{\rm H}$ measured by Kaur et al. (2010) is intrinsic to the system.
References. (1) Sakano et al. 2000; (2) Kaur et al. 2010; (3) Gonzalez et al. 2011; (4) Gonzalez et al. (2012); (5) Jonker et al. (2011).

Facilities: CTIO:1.3m, Blanco, CXO, Swope, NTT, VLT:Melipal

REFERENCES

Alard, C. 2000, A&AS, 144, 363
Alard, C., & Lupton, R. H. 1998, ApJ, 503, 325
Bohlin, R. C., Savage, B. D., & Drake, J. F. 1978, ApJ, 224, 132
Cardelli, J. A., Clayton, G. C., & Mathis, J. S. 1989, ApJ, 345, 245
Casares, J., Charles, P. A., Jones, D. H. P., Rutten, R. G. M., & Callanan, P. J. 1991, MNRAS, 250, 712
Echevarria, J. 1988, MNRAS, 233, 513
Edmonds, P. D., Grindlay, J. E., Cool, A., et al. 1999, ApJ, 516, 250
Fender, R. P., Gallo, E., & Jonker, P. G. 2003, MNRAS, 343, L99
Garcia, M. R., McClintock, J. E., Narayan, R., et al. 2001, ApJL, 553, L47
Gonzalez, O. A., Rejkuba, M., Zoccali, M., Valenti, E., & Minniti, D. 2011, A&A, 534, A3
Gonzalez, O. A., Rejkuba, M., Zoccali, M., et al. 2012, A&A, 543, A13
Grindlay, J. E. 1999, in ASP Conf. Ser. 157, Annapolis Workshop on Magnetic Cataclysmic Variables (San Francisco, CA: ASP), 377
Grindlay, J. E. 2006, AdSpR, 38, 2923
Hameury, J. M., Barret, D., Lasota, J.-P., et al. 2003, A&A, 399, 631
Hynes, R. I., Robinson, E. L., & Jeffrey, E. 2004, ApJ, 608, 101
Ivanova, N., Belczynski, K., Fregeau, J. M., & Rasio, F. A. 2005, MNRAS, 358, 572
Izzo, C., Kornweibel, N., McKay, D., et al. 2004, Msngr, 117, 33
Jonker, P. G., Bassa, C. G., Nelemans, G., et al. 2011, ApJS, 194, 18
Kalogera, V. 1999, ApJ, 521, 723
Kaur, R., Wijnands, R., Paul, B., Patruno, A., & Degenaar, N. 2010, MNRAS, 402, 2388
Lasota, J.-P. 2001, NewAR, 45, 449
Le Fèvre, O., Saisse, M., Mancini, D., et al. 2003, Proc. SPIE, 4841, 1670
Marsh, T. R., Robinson, E. L., & Wood, J. H. 1994, MNRAS, 266, 137
Mauerhan, J. C., Muno, M. P., Morris, M. R., et al. 2009, ApJ, 703, 30
Menou, K., Esin, A. A., Narayan, R., et al. 1999, ApJ, 520, 276
Muno, M. P., Baganoff, F. K., Bautz, M. W., et al. 2003, ApJ, 599, 465
Narayan, R., Garcia, M. R., & McClintock, J. E. 1997, ApJL, 478, L79
Narayan, R., & McClintock, J. E. 2008, NewAR, 51, 733
Patterson, J. 1994, PASP, 106, 209
Pfahl, E., Rappaport, S., & Podsiadlowski, P. 2003, ApJ, 597, 1036
Predehl, P., & Schmitt, J. H. M. M. 1995, A&A, 293, 889
Remillard, R. A., & McClintock, J. E. 2006, ARA&A, 44, 49
Sakano, M., Torii, K., Koyama, K., Maeda, Y., & Yamauchi, S. 2000, PASJ, 52, 1141
Scaringi, S., Bird, A. J., Norton, A. J., et al. 2010, MNRAS, 401, 2207
Schlegel, D. J., Finkbeiner, D. P., & Davis, M. 1998, ApJ, 500, 525
Servillat, M., Grindlay, J., van den Berg, M., et al. 2012, ApJ, 748, 32
Shara, M. M., Hinkley, S., Zurek, D. R., Knigge, C., & Dieball, A. 2005, AJ, 130, 1829
Shaw, R. A. (ed.) 2009, NOAO Data Handbook (Version 1.1; Tucson, AZ: National Optical Astronomical Observatory)
Silber, A. D. 1992, PhD thesis, MIT
Sulkanen, M. E., Brasure, L. W., & Patterson, J. 1981, ApJ, 244, 579
Szkody, P., Gänsicke, B. T., Sion, E. M., & Howell, S. B. 2002, ApJ, 574, 950
Szkody, P., & Henden, A. 2005, JAVSO, 34, 11
Taam, R. E., & Sandquist, E. L. 2000, ARA&A, 38, 113
Terzan, A., & Gosset, E. 1991, A&AS, 90, 451
Udalski, A., Kowalczyk, K., Soszyński, I., et al. 2012, AcA, 62, 133
van den Berg, M., Hong, J. S., & Grindlay, J. E. 2009, ApJ, 700, 1702
Verbunt, F., Bunk, W. H., Ritter, H., & Pfeffermann, E. 1997, A&A, 327, 602
Warner, B. 2003, Cataclysmic Variable Stars, ed. Brian Warner (Cambrige: Cambridge Univ. Press)
Zurita, C., Casares, J., & Shahbaz, T. 2003, ApJ, 582, 369